Two-Dimensional Confinement for Generating Thin Single Crystals for Time-Resolved Electron Diffraction and Spectroscopy: An Intramolecular Proton Transfer Study

Hyein Hwang,[a,b] Vandana Tiwari,[c] Hong-Guang Duan,[d] Simon F. Bittmann,[b] Friedjof Tellkamp,[b] Ajay Jha*[e] and R. J. Dwayne Miller*[f]

a. Department of Chemistry, University of Hamburg, Martin-Luther-King Platz 6, 20146 Hamburg, Germany

b. Max Planck Institute for the Structure and Dynamics of Matter, Luruper Chaussee 149, 22761 Hamburg, Germany

c. European XFEL, Holzkoppel 4, 22869 Schenefeld, Germany

d. Department of Physics, Ningbo University, Ningbo 315211, China

e. The Rosalind Franklin Institute, Rutherford Appleton Laboratory, Harwell Campus, Didcot, Oxfordshire, OX11 OFA, United Kingdom. E-mail: ajay.jha@rfi.ac.uk

f. The Departments of Chemistry and Physics, University of Toronto, 80 St. George Street, Toronto Canada M5S 3H6. E-mail: dmiller@lphys.chem.utoronto.ca

Thin single organic crystals (≤1 μm) with large area (≥100 × 100 μm^2) are desirable to explore their photoinduced processes using transmission-based ultrafast spectroscopy and electron-diffraction techniques. Here we present a method to grow thin large area single crystals of a prototypical proton transfer system, 1,5-dihydroxyanthraquinone. As a proof of concept, we perform optical measurements on as-grown samples and recorded the data in transmission mode.

Although fundamental processes of charge and energy transfer are long standing problems of interest for chemists, it is still extremely challenging to gain a comprehensive mechanistic understanding due to experimental limits in time and space resolution to follow the molecular dynamics. These limits are being overcome as cutting-edge techniques have been developed to capture electronic and structural dynamics accompanying ultrafast (10^{-15} to 10^{-12} second) processes; for example, femtosecond (fs) transient absorption: UV-Vis, X-ray and IR; Raman scattering; X-ray and electron-diffraction based techniques.[1] These developments have now equipped us to investigate intricate excited state processes and their pathways.

Proton transfer is one of the fundamental chemical reactions of interest. It is a key process in many chemical and biological reactions, such as acid-base reaction, photosynthesis and phosphorylation of ADP to ATP.[2] Proton transfer often involves transfer of charge through hydrogen bonds, which is accompanied by structural changes as reorganization in the system and bath. Proton's transfer can be induced when the molecular system is electronically excited, because of charge redistribution in excited states. Excited state proton transfer (ESPT) is known to occur in femtosecond timescales measured using ultrafast spectroscopic methods on various molecular systems: methyl salicylate,[3,4] 2-(2´-hydroxyphenyl) benzothiazole,[5] and hydroxyanthraquinones.[6-10] Most of these time-resolved studies of ESPT dynamics are performed in solution phase. However, ESPT dynamics in the crystalline phase with well-defined spatial relationships is still largely unknown because of the complexity in development of suitable single crystal samples as well as the degree to which proton transfer may be coupled with lattice effect(s). There are new efforts to develop ESPT systems in solid-state as such systems can be employed as optoelectronic devices, such as light emitters [11] or lasing gain media[12,13] utilizing their ultrafast reaction followed by large Stokes shift, or as molecular switch owing to its responsiveness to external stimulation.[14,15] Understanding the role of spatial arrangement of molecular systems in lattices will pave the way towards rationalized tuning of solid-state proton transfer reactions. Our group aims to unravel the

lattice effects in intramolecular proton transfer dynamics in prototypical molecular systems using ultrafast transient absorption and state-of-the-art electron diffraction techniques.

We have chosen 1,5-dihydroxyanthraquinone (1,5-DHAQ) as our model system to study ESPT in crystalline phase. It is known to go through excited state intramolecular proton transfer (ESIPT) by photoexcitation in the visible range, with evidence of dual fluorescence in both solution and crystal phase.[16,17] The ESIPT in 1,5-DHAQ generates a tautomer, in which a proton from one of the hydroxyl groups tunnels to form a covalent bond with adjacent carbonyl oxygen. The potential energy surfaces of 1,5-DHAQ molecule in ethanol in the ground and excited states have been theoretically studied by Zhou et al. to describe the ESIPT mechanism for this system.[18] The inverted energy levels for the two possible tautomers in the excited state and the low energy barrier poise the system to go through an ESIPT process. Towrie et al. used time-resolved infrared spectroscopy on powdered 1,5-DHAQ crystal to decipher different dynamics as compared to solution phase, hinting the role of molecular packing in solid state.[19] To have comprehensive understanding of the ESIPT process in molecular single crystals of 1,5-DHAQ, it is imperative to capture the accompanying electronic and nuclear rearrangements. However, in order to obtain time-resolved structural dynamics, the major limiting step is to obtain large area single crystals, which are thin enough to perform transmission-based optical measurements. Here, we present a method to grow large area crystals using a spatially confined growth mechanism. As-grown single crystals are then studied using fs-transient absorption.

Two-dimensional (2D) spatial confined growth methods are well developed in the field of vapour phase growth of 2D materials, such as graphene or transition metal chalcogenides.[20] Basic knowledge of the method is to confine the space on a substrate for anisotropic crystal growth by modulating the adsorption kinetics. This method is adopted to grow non-layered crystals as well, e.g., perovskite crystal growth in between glass and polymer-covered substrates[21] and further with a seed-printing strategy,[22] and for organic semiconductors grown between overlapped SiO_2/Si

substrates.[23] Namsrai et al. used Hashimoto's vapour phase approach to prepare thin single crystal of 1,5-DHAQ by recrystallizing a thick single crystal melt in the deliberately designed space gap between two quartz plates,[24] but thickness and single-crystal diffraction data of the thin crystals was not presented. Wei et al. prepared 1,5-DHAQ microcrystals using solution drying method. The size of square-like crystals obtained were limited to 2-20 μm.[17] The challenge for femtosecond electron diffraction is to grow near 100 micron to mm area crystals for sufficient sample area for the typical 100 micron spot sizes used for electron probe pulses for sufficient electrons to give high quality diffraction patterns.

In this work, we have exploited stacked muscovite mica sheets to introduce a chemically smooth, confined space, to initiate molecular crystal growth. Muscovite ($KAl_2[AlSi_3O_{10}](OH)_2$) has a layered crystal structure, where layers of negatively charged aluminosilicates are neutralized and weakly bound by potassium ions.[25] Due to its chemically smooth surface and flexibility, muscovite is an attractive substrate for van der Waals epitaxial growth.[26] Also, it is an appropriate substrate for optical studies because it is transparent in the visible and infrared range of the electromagnetic spectrum. Thus, direct optical measurements were available with transmitted beams through the as-grown 1,5-DHAQ crystal on mica.

Figure 1a shows open and confined area of a mica substrate after evaporating 2 ml solution of 1,5-DHAQ in chloroform under room temperature. The confined area refers to the part of the mica sheet covered by another mica sheet. Crystal density was less in the confined area than in open areas of substrates: 34 crystals are counted in a selected area (red rectangular in Fig. 1a, area = 5.26 mm^2) of the confined region, whereas 296 crystals are counted in same area in the open region (blue). Crystal shape is thin and uniform in the closed area, but many bulky crystals are found in the exposed area. The bulky crystals represent the known crystal form of 1,5-DHAQ: prism shape with (100) and (102) faces.[24] We observed the topography of the thin crystals in the confined area with atomic force microscopy (AFM) in intermittent contact mode (Fig. S1). The thicknesses of the thin

crystals are in the range of 1.0 – 1.75 μm. By scanning a corner of a crystal, the stacked layers and incompletely covering top layers are visualized by difference signal image in Fig. 1d (the height profile in Fig. S2). We characterized the cell dimensions of the as obtained crystal by single crystal x-ray diffraction (XRD) at 100 K using Cu x-ray line. The measured cell of our crystal was identical with the cell of DHANTQ02 from the Cambridge Structural Database (CSD) (Table S1).[27] The 1,5-DHAQ molecule has a planar backbone of anthraquinone and two intramolecular hydrogen bonds (1.8 Å) between carbonyl and hydroxyl groups. In the lattice, the molecules form layers through intermolecular hydrogen bonds (2.3 Å) (Fig. 2a). Those layers are stacked by π- π interaction, of which the distance is about 3 Å. The π-stacked layers are stacked along the c axis in an alternative orientation. The angle between the alternative molecular planes ((112) and $(\bar{1}1\bar{2})$, red and green planes in Fig. S3, respectively) is 97.84°. To characterize the plane index of the surface of the thin crystal, we observed the crystals with transmission electron microscopy (TEM) (Fig. 1e). By comparing the d-spacings analysed by selected-area electron diffraction (SAED) pattern on the crystals with reference data,[27] short and long edges are (002) and (110). According to the results, the crystal shape is drawn in Fig. 2b.

The main difference of growth morphology in confined and open areas of mica is crystal density and shape. From classic nucleation theory, the rate of nucleation J, i.e., the number of nuclei formed per unit time per unit volume is described by the Arrhenius reaction velocity equation with the super-saturation, S, to be defined by the Gibbs-Thomson relationship in:

$$J = A \exp\left[-\frac{16\pi\gamma^3\nu^2}{3\mathrm{k}^3T^3(lnS)^2} \right] \quad (1)$$

where γ is the interfacial tension, ν is the molar volume of solute, k is the Boltzmann constant, and T is temperature (°K).[28]

Evaporation of solvent in the confined area is slower than in the open areas, as Berli et al. showed with sessile and confined water droplets,[29] which induces slower increase of S. At a certain time

during evaporation leading to the nucleation step, the supersaturation is lower in the confined space than in the open space; it means that the nucleation barrier is higher in the confined area than in open areas at the same time. Consequently, the crystal growth step proceeds with a smaller number of nuclei. After nucleation, nuclei go through a growth step, which is a kinetic process governed by transport of solute particles, surface diffusion, and equilibrium between adsorption and desorption. The motion of solute particles in a 2D-confined volume of solution during evaporation is supposed to be modified from those in free volume. As Wei et al. modelled crystal morphology for their microdisks under attachment energy equilibrium,[17] thermodynamic modelling is necessary to explain further the growth mechanism of the anisotropic growth in the confined area.

The thin crystals obtained from confined areas are measured for their absorption using a home-built steady state absorption setup. The absorption spectra of crystal and solution sample in acetonitrile are measured and compared to the computed vertical excitation energies with time-dependent density functional theory (TDDFT) methods (Fig. 3a, details are provided in the SI). The absorption edge of the crystal starts around 500 nm, and the first peak of the solution sample is at 430 nm, obtained by the first derivative method. As illustrated in the Highest Occupied Molecular Orbital (HOMO) and Lowest Unoccupied Molecular Orbital (LUMO) diagrams, molecular orbitals are localized in solution whereas they are delocalized over the neighbouring molecular units in crystals (Fig. 3 b, c). Additionally, the broad absorption of the single crystal sample arises from the narrowed gap between the energy levels (Table S3) due to the greater spatial delocalization of the electron distribution.

To quantify the degree of intermolecular interaction, Coulomb coupling of S_0 to S_1 transition dipole moments between two molecules are calculated. The coupling between in-plane neighboring molecules is 303 cm^{-1} and that of π-stacked molecules is 540 cm^{-1} (Fig. S5, Table S5). Thus, the exciton transport should be favoured along the π-stacking direction. Furthermore, these large coupling should influence the photo-induced dynamics, which is studied here using transient absorption

(TA). The excitation energy was 343 nm, and the other specifications of samples and excitation details are listed in Table S6. The TA measurements have been performed in the linear excitation regime with respect to pump-fluence for solution as well as crystals (Fig. S7). First, we examined 1,5-DHAQ solution in acetonitrile (Fig. 4a, b). Excited state absorption (ESA) and stimulated emission (SE) show sharp peaks in spectral profile with long lifetimes. The kinetic trace for the SE (630 nm) is fitted with a bi-exponential function, and that at the ESA (500 nm) band is fitted with a tri-exponential function. SE rises with a time constant of 3.8 ps and decays with lifetime 253 ps. The rising component can be counted as vibrational redistribution in accordance with time-resolved fluorescence studies of 1,8-dihydroxyanthraquinone.[9] The decaying component is assigned to population decay of the excited state.[8] ESA rises with lifetime of 280 fs, which is possibly the proton transfer channel. It decays with a lifetime of 39.7 ps and a long-lived component. The inconsistency of the decay dynamics between SE and ESA indicates the existence of long-lived non-radiative states.[8]

TA spectra of 1,5-DHAQ crystals show broad ESA in between 550 – 800 nm (Fig. 4c). In analogy to the static absorption, this broadness is caused by the manifold of excited states in the crystalline phase. Unlike spectra from solution, emission is rendered undetectable by the presence of overlapping broad absorption band. Fluorescence of 1,5-DHAQ microcrystals was observed between 575 – 725 nm.[17] The differential absorption spectral profile shows a peak at around 565 nm at early delay times (<1 ps) and there is a longer-lived species at around 670 nm. The kinetic traces of these two peaks show different decay dynamics. Kinetic trace at 565 nm is fitted with a bi-exponential function, on the other hand, the trace at 670 nm is better fit with a tri-exponential function (Fig. 4d, Table S7). At early times, both the peaks have sub-picosecond decay components. But the ESA at 670 nm has an additional longer-lived component of 9.2 ps as excited state lifetime. Dispersed 1,5-DHAQ microcrystals showed sub-nanoseconds long fluorescence lifetime, while an emission peak at 575 nm had an additional fast decaying component of 1.4 ps.[17] Authors inferred

this picosecond decay to be evidence of the proton transfer pathway, as the sub-nanosecond decay is from fluorescence. However, from our observations, there is a sub-picosecond decay component of the excited state, which can be conjectured to be the proton transfer step.

The ground state intramolecular hydrogen bond lengths are 1.796 Å and 2.234 Å in the lattice and in acetonitrile, respectively. This significant difference means that 1,5-DHAQ will not only have different bath interactions in single crystals but will also have distinct intramolecular structural parameters. Since ESIPT is coupled to skeletal modes of its system, molecular packing in the crystal can modify or diversify the reaction pathways for ESIPT.[15] Towrie et al. studied transient vibrational changes of the C=O stretching mode in solution and ground crystal of 1,5-DHAQ to suggest quenching of the ESIPT channel in the presence of additional energy dissipation pathways, or stronger lattice coupling, in the crystalline state.[19] Additionally, the first excitation level of the crystal form is lowered than that of solution due to the lattice interaction. Thus, the pump energy used in the TA experiments for the single crystal is much above the absorption edge compared to solution phase. The excess energy can dissipate through the vibrational manifolds of the excited states, where the gaps between the electronic states are reduced relative to the solution phase, isolated molecular case. To further discuss the energy relaxation pathways, the details of the energy diagram and photoreaction dynamics for single crystals are needed, requiring additional computational effort. Furthermore, direct ultrafast electron diffraction studies of the structural changes in this molecular crystal are necessary to correlate to the electronic information in this work.

In summary, we demonstrated here a 2D confined growth method using dispersed muscovite mica sheets in saturated solution, which can be used to grow large area crystals of 1,5-DHAQ with thickness 1 to 1.75 μm. These crystals are optically thin enough to perform ultrafast transient spectroscopic measurements on as-grown crystals. We have successfully performed transient absorption measurements on as-grown crystals, which reveal significantly modified proton transfer

dynamics and relaxation processes as compared to the solution phase. Quantum calculations on this system reveal the role of excitonic coupling in modifying the excited state picture of this molecular system in crystalline phase, which is a direct manifestation of various stacking interaction in the single crystal state. Our future studies will focus on understanding the role of excitonic coupling on proton transfer dynamics. Here, one can imagine that the spatial delocalization of the excitation due to the excitonic coupling will reduce the gradients in the electron distribution driving the proton transfer. This system was specifically designed to study this problem using ultrabright electron sources to directly observe the relevant atomic motions guiding proton transfer. This work provides the essential excited state dynamics and shows that these process in single crystals are photo-reversible, which will greatly enhance the signal to noise in signal averaging diffraction data. By comparison to the dynamics in solution phase, the degree of excitonic coupling and specific effects on the proton transfer process can be directly determined. We envision that our crystal growth method can be extended to other molecular systems as well.

Conflicts of interest

There are no conflicts to declare.

References

1. A. A. Ischenko, P. M. Weber and R. J. D. Miller, *Chem. Rev.*, 2017, **117**, 11066-11124.
2. O. K. Volkhard May, in *Charge and Energy Transfer Dynamics in Molecular Systems*, 2003, pp. 377-403.
3. K. K. Smith and K. J. Kaufmann, *J. Phys. Chem.*, 2002, **85**, 2895-2897.
4. J. L. Herek, S. Pedersen, L. Bañares and A. H. Zewail, *J. Chem. Phys.*, 1992, **97**, 9046-9061.
5. F. Laermer, T. Elsaesser and W. Kaiser, *Chem. Phys. Lett.*, 1988, **148**, 119-124.
6. J. A. Berenbeim, S. Boldissar, S. Owens, M. R. Haggmark, G. Gate, F. M. Siouri, T. Cohen, M. F. Rode, C. S. Patterson and M. S. de Vries, *Sci. Adv.*, 2019, **5**, eaaw5227.
7. C. Muller, J. Schroeder and J. Troe, *J. Phys. Chem. B*, 2006, **110**, 19820-19832.
8. O. F. Mohammed, D. Xiao, V. S. Batista and E. T. Nibbering, *J. Phys. Chem. A*, 2014, **118**, 3090-3099.
9. S. Y. Arzhantsev, S. Takeuchi and T. Tahara, *Chem. Phys. Lett.*, 2000, **330**, 83-90.
10. J. Jethwa, D. Ouw, K. Winkler, N. Hartmann and P. Vöhringer, *Z. Phys. Chem.*, 2000, **214**.
11. V. S. Padalkar and S. Seki, *Chem. Soc. Rev.*, 2016, **45**, 169-202.
12. C.-C. Yan, X.-D. Wang and L.-S. Liao, *ACS Photonics*, 2020, **7**, 1355-1366.

13. J.-J. Wu, H. Gao, R. Lai, M.-P. Zhuo, J. Feng, X.-D. Wang, Y. Wu, L.-S. Liao and L. Jiang, *Matter*, 2020, **2**, 1233-1243.
14. W. Wang, M. Marshall, E. Collins, S. Marquez, C. Mu, K. H. Bowen and X. Zhang, *Nat. Commun.*, 2019, **10**, 1170.
15. S. Khatib, M. Botoshansky and Y. Eichen, *Acta Crystallogr. Sect. B: Struct. Sci.*, 1997, **53**, 306-316.
16. M. H. Van Benthem and G. D. Gillispie, *J. Phys. Chem.*, 1984, **88**, 2954-2960.
17. G.-Q. Wei, Y. Yu, M.-P. Zhuo, X.-D. Wang and L.-S. Liao, *J. Mater. Chem. C*, 2020, **8**, 11916-11921.
18. Q. Zhou, C. Du, L. Yang, M. Zhao, Y. Dai and P. Song, *J Phys Chem A*, 2017, **121**, 4645-4651.
19. M. Towrie, A. W. Parker, K. L. Ronayne, K. F. Bowes, J. M. Cole, P. R. Raithby and J. E. Warren, *Appl. Spectrosc.*, 2009, **63**, 57-65.
20. S. Zhou, L. Gan, D. Wang, H. Li and T. Zhai, *Nano Research*, 2018, **11**, 2909-2931.
21. Z. Chen, Q. Dong, Y. Liu, C. Bao, Y. Fang, Y. Lin, S. Tang, Q. Wang, X. Xiao, Y. Bai, Y. Deng and J. Huang, *Nat. Commun.*, 2017, **8**, 1890.
22. Z. Gu, Z. Huang, C. Li, M. Li and Y. Song, *Sci. Adv.*, 2018, **4**, eaat2390.
23. Y. Shi, L. Jiang, J. Liu, Z. Tu, Y. Hu, Q. Wu, Y. Yi, E. Gann, C. R. McNeill, H. Li, W. Hu, D. Zhu and H. Sirringhaus, *Nat. Commun.*, 2018, **9**, 2933.
24. N. Namsrai, T. Yoshinari, H. Itoh, S.-i. Nagasaka, Y. Kuriyama, M. Sakamoto and Y. Takahashi, *J. Phys. Soc. Jpn.*, 2006, **75**, 044703.
25. C. R. A. C. David R. Collins, *Am. Mineral.*, 1992, **77**, 1172-1181.
26. M. Yen, Y. Bitla and Y.-H. Chu, *Mater. Chem. Phys.*, 2019, **234**, 185-195.
27. P. A. B. Marasinghe and G. D. Gillispie, *Acta Crystallogr. C Struct.*, 1993, **49**, 113-114.
28. J. W. Mullin, *Crystallization*, Butterworth-Heinemann, 4 edn., 2001.
29. C. L. A. Berli and M. G. Bellino, *Adv. Mater. Interfaces*, 2020, **8**, 2002098.

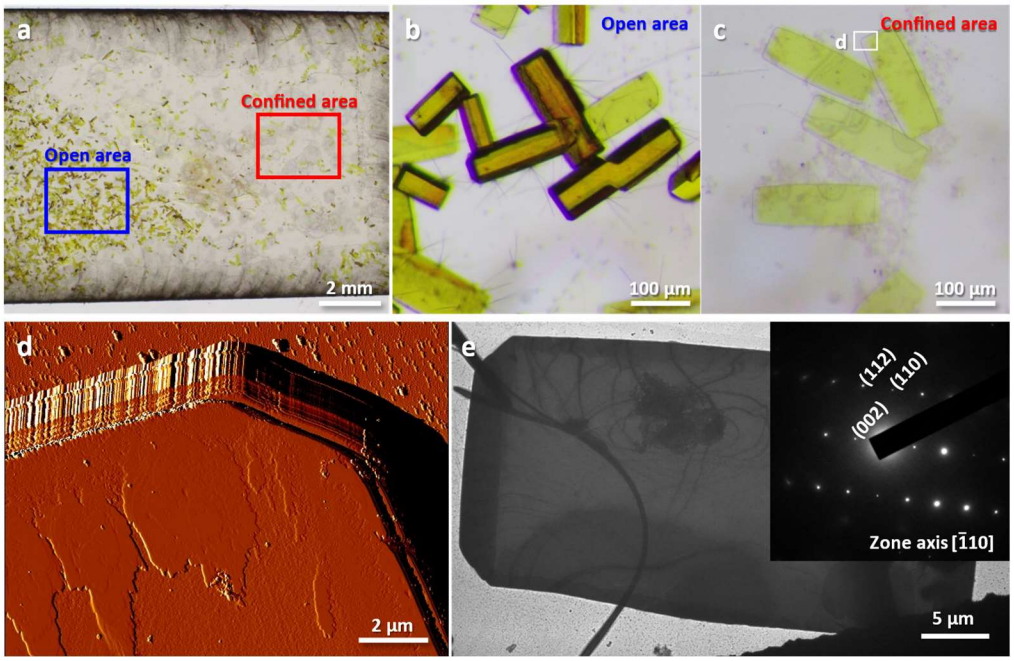

Figure 1. Morphology of 1,5-DHAQ crystals grew on muscovite mica substrate. (a) Optical image of full coverage of a substrate. (b) Enlarged images in open area and (c) in confined area. (d) Error signal image of a crystal measured by AFM within the area marked in white line rectangular in (c). (e) Bright field TEM image of 15HAQ crystal. Inset: SAED pattern indexing with zone axis [$\bar{1}10$].

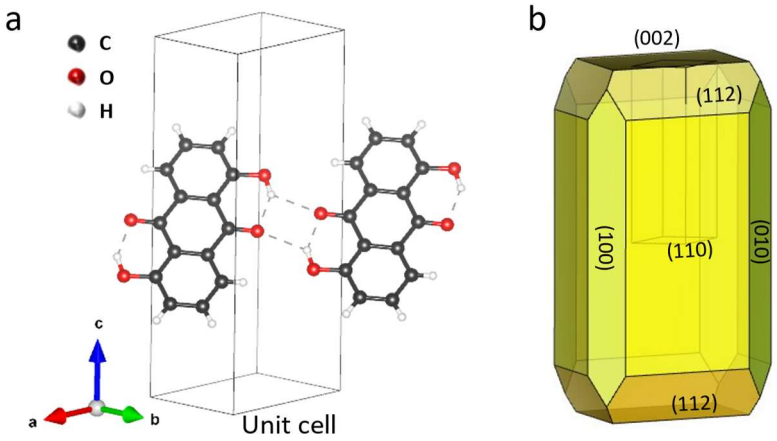

Figure 2. Crystal structure and shape model of 1,5-DHAQ. (a) Two 1,5-DHAQ molecules forming intermolecular hydrogen bond in a unit cell. Dashed lines indicate hydrogen bonds. (b) Illustration of crystal shape.

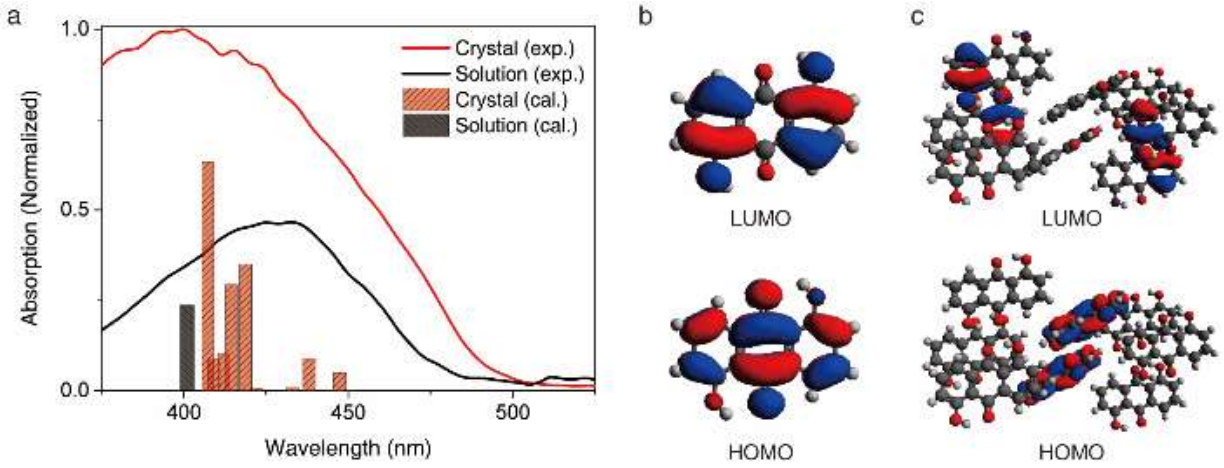

Figure 4. Optical measurements of 1,5-DHAQ single crystal. (a) Lines: Steady-state absorption spectrum of crystal and solvent sample. Bars: calculated value of excitation energies by TDDFT method. The height is oscillator strength in relative value (absolute values in Table S3). Data in a broader spectral range is given in Fig. S4. (b, c) HOMO and LUMO of 1,5-DHAQ in solution and crystal, respectively.

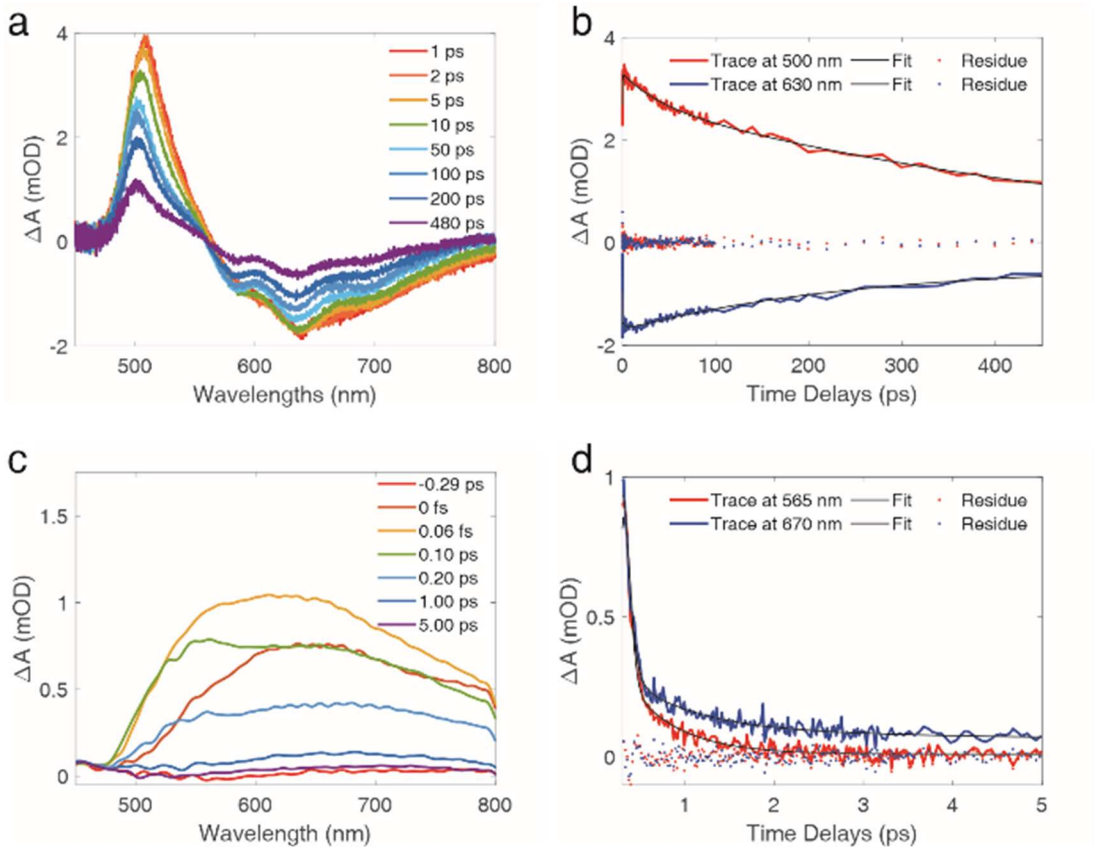

Figure 3. Transient absorption measurements of 1,5-DHAQ. Spectral profile and kinetic traces at selected wavelengths of solution (a, b) and crystal (c, d). Pump wavelength used is 343 nm.

Supporting Information

Two-Dimensional Confinement for Generating Thin Single Crystals for Time-Resolved Electron Diffraction and Spectroscopy: An Intramolecular Proton Transfer Study

Hyein Hwang,[a,b] Vandana Tiwari,[c] Hong-Guang Duan,[d] Simon F. Bittmann,[b] Friedjof Tellkamp,[b] Ajay Jha*[e] and R. J. Dwayne Miller*[f]

[a] Department of Chemistry, University of Hamburg, Martin-Luther-King Platz 6, 20146 Hamburg, Germany.

[b] Max Planck Institute for the Structure and Dynamics of Matter, Center for Free Electron Laser Science, Luruper Chaussee 149, 22761 Hamburg, Germany.

[c] European XFEL, Holzkoppel 4, 22869 Schenefeld, Germany.

[d] Department of Physics, Ningbo University, Ningbo 315211, China.

[e] The Rosalind Franklin Institute, Rutherford Appleton Laboratory, Harwell Campus, Didcot, Oxfordshire, OX11 OFA, United Kingdom. E-mail: ajay.jha@rfi.ac.uk

[f] The Departments of Chemistry and Physics, University of Toronto, 80 St. George Street, Toronto Canada M5S 3H6. E-mail: dmiller@lphys.chem.utoronto.ca

Table of Contents

Materials and Methods

Materials

1,5-Dihydroxyanthraquinone (1,5-DHAQ, technical grade, > 85%) and chloroform (analytical standard) were purchased from Sigma-Aldrich. V-1 grade 0.26 mm muscovite mica block was purchased from Sungil Industries. Mica is cut and cleaved into proper dimension (edge length 10 to 15 mm and thickness around 0.2 mm) to soak in a 20 ml vial.

Crystallization

Mica sheets were heated at 105 °C for 10 minutes on hot plate and rinsed with acetone to remove surface impurities. They are soaked in a vial containing 2 mL of 83 mM solution of 1,5-DHAQ in chloroform. The vial is closed with its lid and heated for 10 minutes at 60 °C, which is slightly above the boiling point of chloroform. Then we kept the temperature of the hot plate at 40 °C and left it for 10 minutes, and then brought the vial to room temperature. We opened the lid after 10 minutes and covered it with aluminum foil with one pin hole made by 0.8 mm needle. The vial was left in stable place for a few days for solvent to completely evaporate. To prepare samples for Transmission electron microscope (TEM), we put carbon film coated TEM grid on a mica sheet in the batch of crystallization. Crystals having same shape as those on mica sheet grew on the carbon film.

Characterizations

Optical images are taken by Olympus SZX10 with DP27 camera and analyzed by Stream Basic software and ImageJ. Crystal topography was observed with NanoWizard® 4 XP BioScience Atomic force microscope (AFM) in intermittent contact mode [1]. X-ray diffraction (XRD) was measured with 4-Circle Single Crystal Diffractometer SuperNova from Oxford Diffraction. Transmission electron microscopy (TEM) data are taken with CryoTEM JEOL JEM-2100F. We used carbon film coated 200 mesh Copper grid. Crystal structure analysis and powder diffraction pattern simulation was performed with VESTA. TEM images are analyzed with Gatan DigitalMicrograph.

Steady state absorption measurements

Steady state absorption measurements of solution and crystals have been performed on a home-built absorption spectrophotometer. Light sources employed in the set-up are deuterium and halogen lamps, which provide white light in the range of 215 – 2500 nm. The transmitted light is collected by spectrometer (Avantes, AvaSpec-ULS2048-USB2-UA-50). To measure absorption spectra, crystals are placed on a quartz substrate attached on a lens mount and solution sample is contained in a 1 mm quartz cuvette. Absorption spectrum is plotted as the logarithm of transmitted spectrum through the bare substrate or pure solvent divided by that through a crystal on substrate or solution sample.

Femtosecond Transient absorption measurements

Transient absorption measurements of 1,5-DHAQ in solution and crystalline form have been performed on a home-built transient absorption (TA) set up. The details of the setup have been described previously [2]. Briefly, the TA setup uses Nd based commercial laser, PHAROS by Light conversion. The fundamental beam wavelength is 1030 nm with output power of 1 W at the repetition rate of 1 kHz. The fundamental laser beam is divided to pump and probe beams using a beam splitter: 20% of the beam is guided to focus on a 3 mm YAG crystal to generate a white light as probe beam, and the remaining 80% of fundamental beam is directed to generate 343 nm pump beam using third harmonic generation process. The pump beam is chopped using a Thorlabs chopper operating at 500 Hz, and the pump energy is controlled using set of neutral density filters. The diameters of pump and probe beams at the sample position are 190 μm and 100 μm, respectively. Time delay between pump and probe is controlled by 150 mm linear motorized delay stage from Newport. Probe spectra for each time-delay are detected with the combination of a spectrograph (9055, Sciencetech) and a charge-coupled device linear image sensor (CCD; S11156-2048-02, Hamamatsu Photonics). All the experiments were performed under room temperature. The concentration of the solution sample was 80 μM. Time-resolved absorption spectra were measured with ~200-fs time resolution. Transient absorption data were analysed with Python GUI coded by Simon Bittmann.

Calculation and data analysis

The vertical excitation energies are calculated with time-dependent density functional theory (TDDFT) using Gaussian 09 package [3]. We adopted coordinates of 8 1,5-DHAQ molecules in a unit cell from CIF file of DHANTQ02 [4] posted at Cambridge Structural Database as crystal model. The geometries of crystal and solution model were optimized at B3LYP/6-31G and B3LYP/6-31G(d) level, respectively. Coulomb coupling between transition dipole moments of two molecules was calculated by Fortran code written by Hong-Guang Duan.

Supporting Figures and Tables

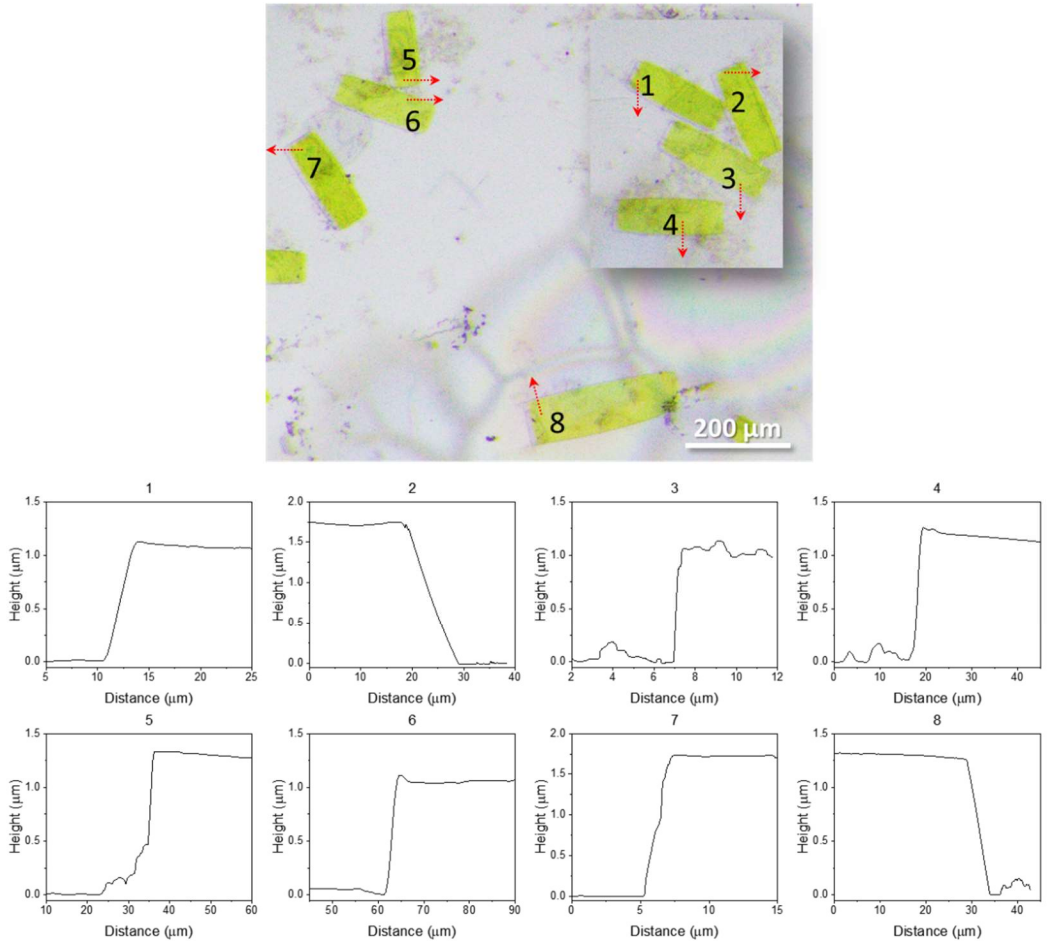

Figure S5. Height profiles at the edges of each crystal by AFM. Red arrows represent tracing direction.

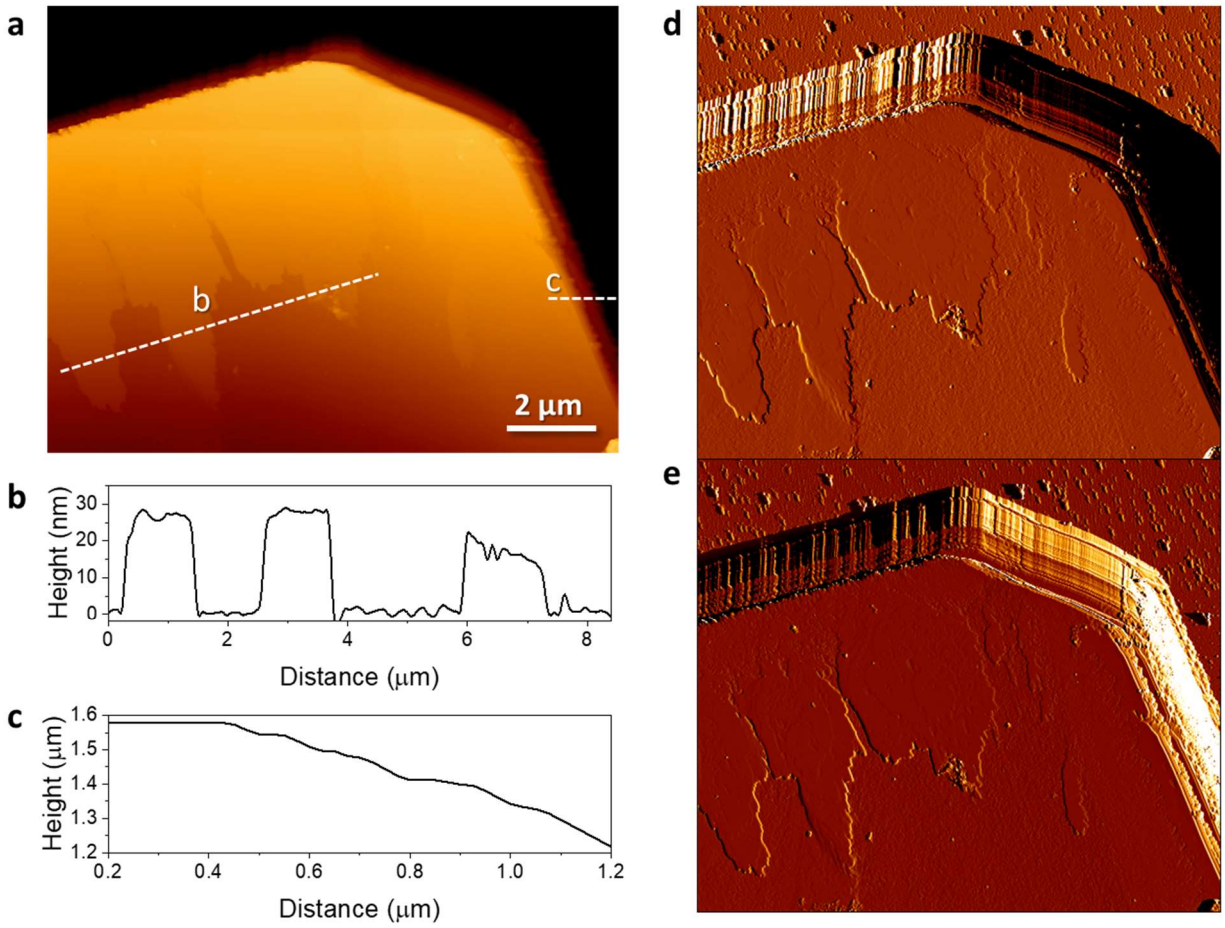

Figure S6. Topography of 1,5-DHAQ thin crystal. (a) AFM height image. (b, c) Height profile. Each profile is traced along the dashed lines in (a) correspondingly. The background of surface is subtracted in profile (b). (d, e) Error signal image of trace and retrace, respectively.

Table S1. Lattice parameters of 1,5-DHAQ **[4].**

Crystal system	Monoclinic
Space group (point group)	$P2_1/c$
a (Å)	6.0092(5)
b (Å)	5.3074(2)
c (Å)	15.7538(6)
α (deg)	90
β (deg)	93.672(5)
γ (deg)	90

Table S2. D-spacing of crystal planes shown in Fig. 1e. Calculation with reference data and analysis with selected area electron diffraction (SAED) pattern by TEM.

h	k	l	d (Å), Calculated	d (Å), Analyzed
0	0	2	7.86	7.38
1	1	0	3.97	4.15
1	1	2	3.49	3.62

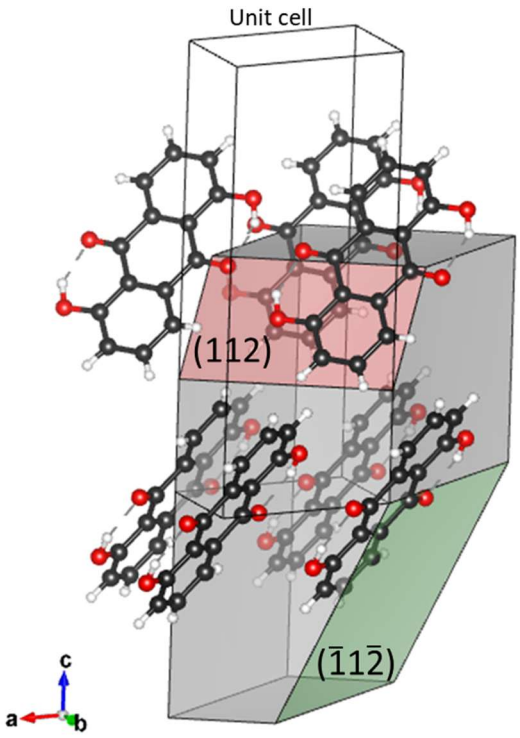

Figure S7. **Illustration of crystallographic planes go through molecular planes.** Red plane (112) represents the face of upper stacks of molecules in the figure, and green plane $(\bar{1}1\bar{2})$ represents the molecular planes of lower stacks. Grey planes are arbitrary planes.

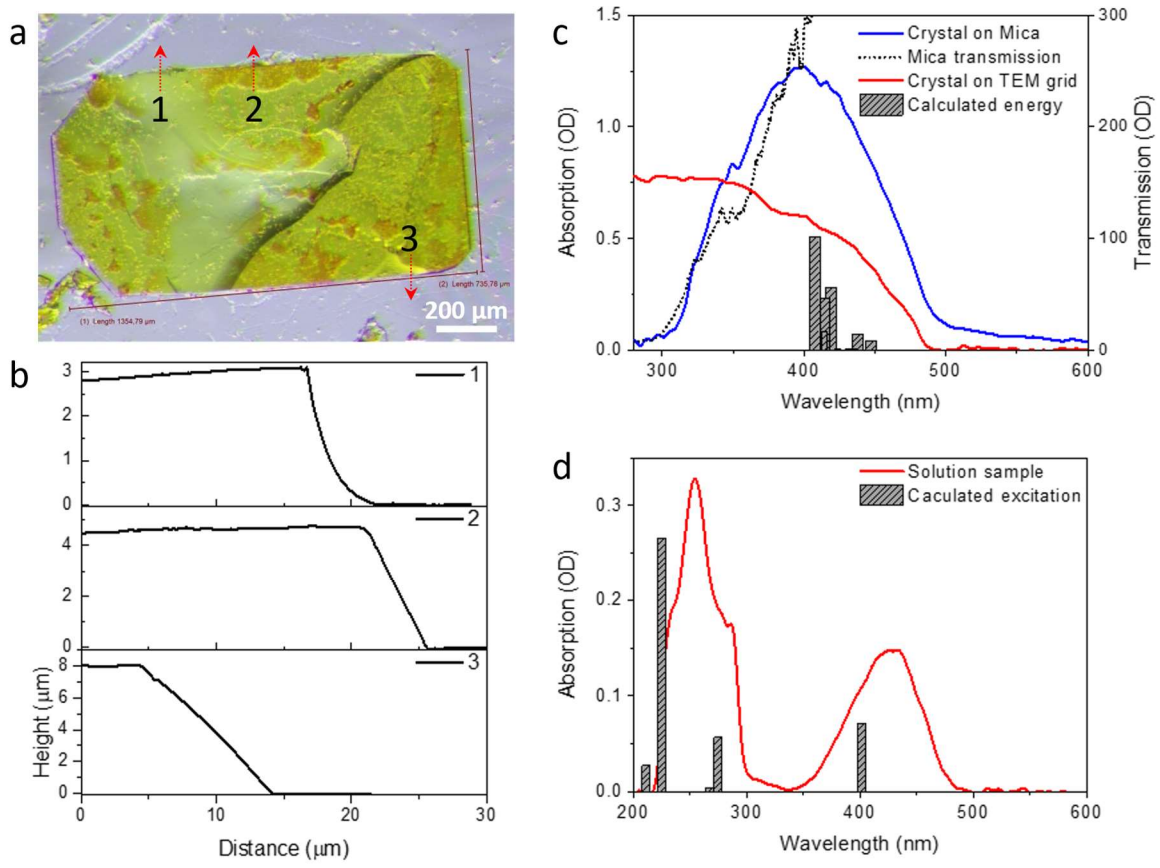

Figure S8. Characterization of TA-measured samples. (a) Optical image of 1,5-DHAQ crystal used for TA measurement. (b) Height profile measured by AFM. Traced line is marked with red arrow in (a) correspondingly. (c) Absorption spectrum 1,5-DHAQ crystal. Spectrum of crystal on mica (blue line) is cut off below 300 nm due to opaqueness of mica in UV region. Dotted line is transmission spectrum measured at mica substrate. Spectrum of crystal on TEM grid (red line) shows continuous absorption below 300 nm. Columns are positioned at the wavelengths of the calculated excitation energies with heights representing relative oscillator strength. (d) Absorption spectra of 1,5-DHAQ solution in acetonitrile. Columns represent the calculated energies with relative oscillator strengths. The values of calculated excitation energies and corresponding oscillator strengths are listed in Table S3.

Table S3. Calculated electronic excited state energies and oscillator strengths of 1,5-DHAQ crystal and solution.

	Excited state*	Excitation energy (nm)	Oscillator strength
Crystal	1	449.01	0.0007
	3	447.30	0.0197
	6	438.10	0.0356
	8	433.02	0.0034
	10	422.25	0.0027
	12	418.76	0.1403
	14	414.48	0.1174
	16	412.20	0.0415
	18	409.11	0.0346
	20	407.40	0.2534
Solution	1	401.00	0.2365
	6	274.59	0.1902
	8	266.85	0.0148
	13	224.78	0.8851
	14	224.64	0.0005
	18	210.92	0.0924
	20	205.32	0.0001

*States with oscillator strength equal to zero are omitted.

Table S4. Transitions contribute to the first excitation.

	Transition	Amplitude
Crystal	HOMO-3 → LUMO	0.13166
	HOMO-1 → LUMO+1	0.31358
	HOMO → LUMO	0.52727
	HOMO → LUMO+2	-0.27189
Solution	HOMO → LUMO	0.70262

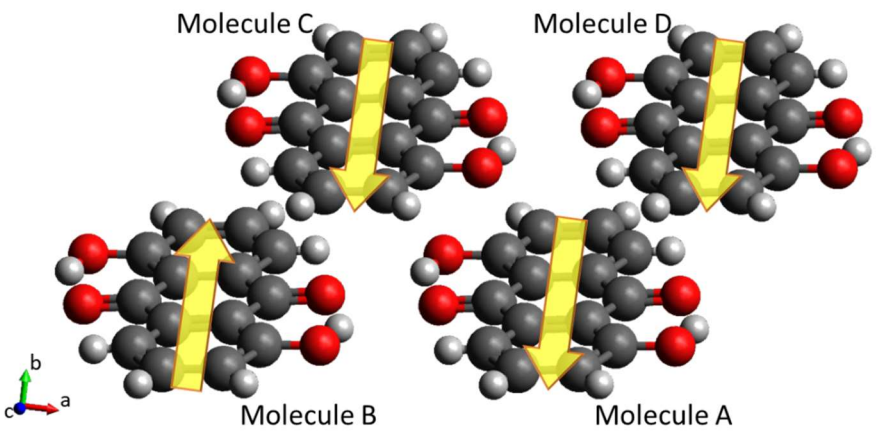

Figure S9. $S_0 \rightarrow S_1$ Transition dipole moments of 1,5-DHAQ molecules. The direction of the dipole moment is depicted with yellow arrows.

Table S5. Calculated intermolecular Coulomb coupling between the transition dipole moments depicted in Fig. S5.

Molecule B ↔ Molecule A	-302.73 cm^{-1}
Molecule C ↔ Molecule A	382.86 cm^{-1}
Molecule D ↔ Molecule A	539.78 cm^{-1}

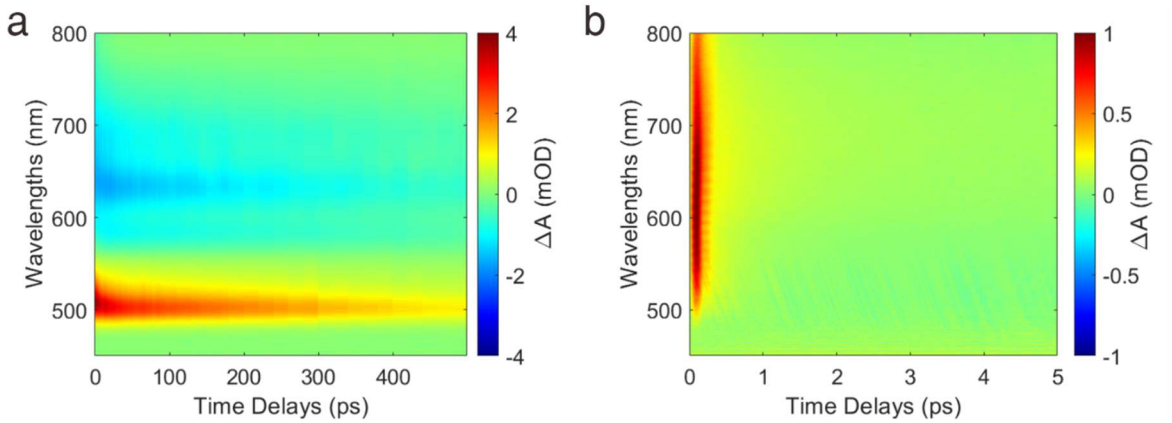

Figure S10. 2-dimensional color plot of transient absorption spectra of 1,5-DHAQ. (a) Solution and (b) crystal.

Table S6. Specifications of crystal and solution samples measured transient absorption.

	Crystal	Solution
Absorbance at 343 nm	0.84 OD	0.078 OD
Density (crystal)	1.51 $g \cdot cm^{-3}$ [4]	
Thickness (crystal)	3.88 – 8.00 µm	
Concentration (solution)		$7.96 \cdot 10^{-8}$ $mol \cdot cm^{-3}$
Fluence	1.1 $mJ \cdot cm^{-2}$	2.7 $mJ \cdot cm^{-2}$
Cross-section	$2.63 \cdot 10^{-19}$ – $7.02 \cdot 10^{-19}$ cm^2	$1.63 \cdot 10^{-16}$ cm^2
Excitation fraction	0.05 – 0.14 %	7.68 %

Table S7. Time components of the kinetic traces in Fig. 4 given with exponential fit parameters and physical assignments on the components.

	Wavelength	τ_1 (ps) / Assignment	τ_2 (ps) / Assignment	τ_3 (ps) / Assignment
Solution	**500 nm**	0.279 ± 0.014 (rise) Proton transfer	40 ± 11 Non-radiative decay	> 500 S_1 state decay
	630 nm	3.8 ± 1.7 (rise) Vibrational redistribution	250 ± 50 S_1 state decay	
Crystal	**565 nm**	< 0.2	0.56 ± 0.06 Vibrational redistribution	
	670 nm	< 0.2	0.78 ± 0.20 Vibrational redistribution	9 ± 5 S_1 state decay

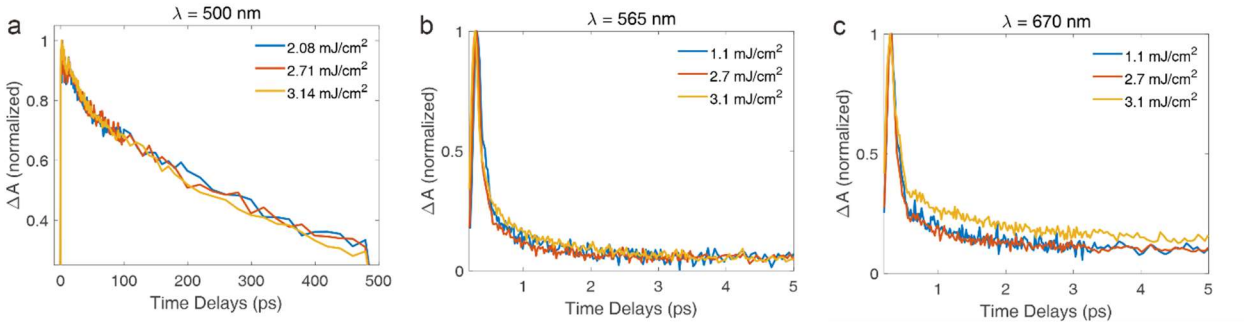

Figure S11. Photon fluence dependence. Normalized kinetic traces of 1,5-DHAQ solution with different photon fluence at 500 nm (a) and crystal at 565 nm (b) and 670 nm (c).

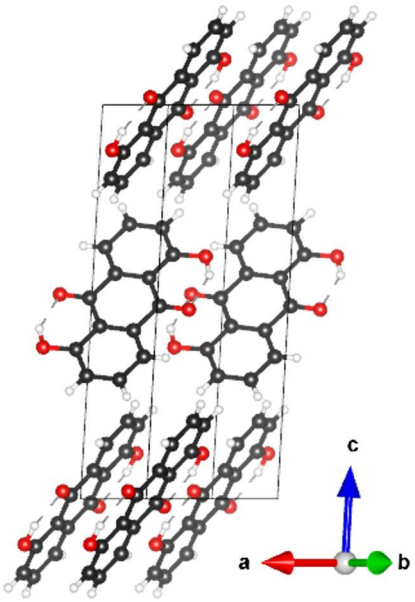

Figure S12. 1,5-DHAQ crystal model containing 8 molecules in a unit cell used for electronic excitation calculation.

Table S8. Coordinates of input files for electronic excitation calculation.

	X	Y	Z
O	2.866014	4.284133	1.812999
O	2.134240	1.023267	13.908460
O	2.638713	1.630433	6.047731
O	2.361542	3.676967	9.673728
O	1.885403	1.879350	0.304053
O	3.114851	3.428050	15.417405
O	3.619324	4.533050	7.556676
O	1.380931	0.774350	8.164782
C	3.866127	5.174715	1.894436
C	1.134127	0.132685	13.827023
C	1.638600	2.521015	5.966294
C	3.361655	2.786385	9.755165
C	3.832780	0.774350	2.947773
C	1.167474	4.533051	12.773685
C	1.671947	3.428050	4.912956
C	3.328308	1.879350	10.808503
C	4.815314	1.712167	3.097127
C	0.184940	3.595233	12.624331
C	0.689413	4.365867	4.763602
C	4.310842	0.941533	10.957856
C	-0.138340	1.792840	2.183711
C	5.138594	3.514560	13.537748
C	5.643067	4.446540	5.677019
C	-0.642812	0.860860	10.044440
C	5.916524	0.907035	1.135089
C	-0.916269	4.400366	14.586369
C	-0.411797	3.560735	6.725640
C	5.412051	1.746665	8.995819
C	4.923783	5.231504	0.966870
C	0.076471	0.075896	14.754589
C	0.580944	2.577804	6.893860

C	4.419310	2.729596	8.827599
C	1.030704	1.009468	0.157215
C	3.969551	4.297933	15.564244
C	4.474023	3.663168	7.703515
C	0.526231	1.644233	8.017944
H	3.095066	0.705884	3.553050
H	1.905189	4.601516	12.168409
H	2.409661	3.359584	4.307680
H	2.590593	1.947816	11.413779
H	0.505723	2.425482	2.232447
H	4.494531	2.881918	13.489011
H	4.999004	5.079182	5.628282
H	0.001251	0.228218	10.093176
H	4.811590	2.292797	3.773150
H	0.188664	3.014603	11.948309
H	0.693137	4.946497	4.087579
H	4.307118	0.360903	11.633879
H	3.008102	3.736410	1.069059
H	1.992153	1.570990	14.652399
H	2.496625	1.082710	6.791670
H	2.503629	4.224691	8.929788
C	3.832780	6.081750	2.947773
C	1.167474	-0.774350	12.773685
C	3.866127	-0.132685	1.894436
C	1.134127	5.440085	13.827023
C	5.870860	1.792840	2.183711
C	-0.870606	3.514560	13.537748
C	-0.366133	4.446540	5.677019
C	5.366388	0.860860	10.044440
C	-0.092676	0.907035	1.135089
C	-1.193886	1.712167	3.097127
C	6.194140	3.595233	12.624331
C	5.092931	4.400366	14.586369

C	6.698613	4.365867	4.763602
C	5.597404	3.560735	6.725640
C	-0.597149	1.746665	8.995819
C	-1.698359	0.941533	10.957856
C	4.923783	-0.075896	0.966870
C	7.039904	1.009468	0.157215
C	-2.039649	4.297933	15.564244
C	0.076471	5.383296	14.754589
C	-1.535177	3.663168	7.703515
C	6.535431	1.644233	8.017944
C	4.978496	4.297933	-0.157215
C	5.916524	6.214435	1.135089
C	-0.916269	-0.907035	14.586369
C	0.021759	1.009468	15.878673
C	1.085417	0.075896	-0.966870
C	3.914838	5.231504	16.688328
H	3.095066	6.013284	3.553050
C	4.815314	7.019568	3.097127
C	0.184940	-1.712167	12.624331
H	1.905189	-0.705884	12.168409
O	2.866014	-1.023267	1.812999
O	2.134240	6.330667	13.908460
H	6.514923	2.425482	2.232447
H	-1.514669	2.881918	13.489011
H	-1.010196	5.079182	5.628282
H	6.010451	0.228218	10.093176
C	-1.085417	-0.075896	0.966870
C	-2.176420	0.774350	2.947773
H	-1.197610	2.292797	3.773150
H	6.197864	3.014603	11.948309
C	7.176674	4.533051	12.773685
C	6.085672	5.383296	14.754589
C	7.681147	3.428050	4.912956

H	6.702337	4.946497	4.087579
C	6.590144	2.577804	6.893860
C	-1.589890	2.729596	8.827599
H	-1.702082	0.360903	11.633879
C	-2.680893	1.879350	10.808503
C	4.978496	-1.009468	-0.157215
C	7.094617	0.075896	-0.966870
O	7.894604	1.879350	0.304053
O	-2.894349	3.428050	15.417405
C	-2.094362	5.231504	16.688328
C	0.021759	6.316868	15.878673
O	-2.389876	4.533050	7.556676
O	7.390131	0.774350	8.164782
O	4.123797	3.428050	-0.304053
C	6.101876	4.400366	-1.135089
C	7.039904	6.316868	0.157215
C	5.870860	7.100240	2.183711
C	-0.870606	-1.792840	13.537748
C	-2.039649	-1.009468	15.564244
C	-1.101622	0.907035	16.856548
O	0.876458	1.879350	16.025511
C	0.092676	-0.907035	-1.135089
C	2.143073	0.132685	-1.894436
C	2.857182	5.174715	17.615894
C	4.907578	6.214435	16.856548
H	4.811590	7.600197	3.773150
H	0.188664	-2.292797	11.948309
H	3.008102	-1.570990	1.069059
H	1.992153	6.878391	14.652399
C	-2.143073	-0.132685	1.894436
C	-1.030704	-1.009468	-0.157215
H	-2.914134	0.705884	3.553050
H	7.914389	4.601516	12.168409

C	7.143327	5.440085	13.827023
C	6.030959	6.316868	15.878673
H	8.418861	3.359584	4.307680
C	7.647800	2.521015	5.966294
C	-2.647546	2.786385	9.755165
H	-3.418607	1.947816	11.413779
O	4.123797	-1.879350	-0.304053
C	6.101876	-0.907035	-1.135089
C	8.152273	0.132685	-1.894436
C	-3.152018	5.174715	17.615894
C	-1.101622	6.214435	16.856548
O	0.876458	7.186751	16.025511
C	6.147540	3.514560	-2.183711
C	7.094617	5.383296	-0.966870
O	7.894604	7.186751	0.304053
H	6.514923	7.732882	2.232447
H	-1.514669	-2.425482	13.489011
O	-2.894349	-1.879350	15.417405
C	-2.094362	-0.075896	16.688328
C	-1.147285	1.792840	17.905169
C	0.138340	-1.792840	-2.183711
C	2.176420	-0.774350	-2.947773
O	3.143186	1.023267	-1.812999
O	1.857069	4.284133	17.534457
C	2.823835	6.081750	18.669232
C	4.861915	7.100240	17.905169
O	-3.143186	-1.023267	1.812999
O	-1.885403	-1.879350	-0.304053
O	8.143440	6.330667	13.908460
O	6.885658	7.186751	16.025511
O	8.647913	1.630433	6.047731
O	-3.647659	3.676967	9.673728
C	6.147540	-1.792840	-2.183711

C	8.185620	-0.774350	-2.947773
O	9.152386	1.023267	-1.812999
O	-4.152131	4.284133	17.534457
C	-3.185365	6.081750	18.669232
C	-1.147285	7.100240	17.905169
H	5.503477	2.881918	-2.232447
C	7.203086	3.595233	-3.097127
C	8.152273	5.440085	-1.894436
C	-3.152018	-0.132685	17.615894
C	-2.202831	1.712167	18.818586
H	-0.503222	2.425482	17.953906
H	-0.505723	-2.425482	-2.232447
C	1.193886	-1.712167	-3.097127
H	2.914134	-0.705884	-3.553050
H	3.001098	1.570990	-1.069059
H	1.999157	3.736410	16.790518
H	2.086121	6.013284	19.274508
C	3.806369	7.019568	18.818586
H	5.505978	7.732882	17.953906
H	-3.001098	-1.570990	1.069059
H	8.001353	6.878391	14.652399
H	8.505825	1.082710	6.791670
H	-3.505571	4.224691	8.929788
H	5.503477	-2.425482	-2.232447
C	7.203086	-1.712167	-3.097127
H	8.923334	-0.705884	-3.553050
H	9.010298	1.570990	-1.069059
H	-4.010043	3.736410	16.790518
H	-3.923080	6.013284	19.274508
C	-2.202831	7.019568	18.818586
H	-0.503222	7.732882	17.953906
H	7.206810	3.014603	-3.773150
C	8.185620	4.533051	-2.947773

O	9.152386	6.330667	-1.812999
O	-4.152131	-1.023267	17.534457
C	-3.185365	0.774350	18.669232
H	-2.206555	2.292797	19.494608
H	1.197610	-2.292797	-3.773150
H	3.802645	7.600197	19.494608
H	7.206810	-2.292797	-3.773150
H	-2.206555	7.600197	19.494608
H	8.923334	4.601516	-3.553050
H	9.010298	6.878391	-1.069059
H	-4.010043	-1.570990	16.790518
H	-3.923080	0.705884	19.274508

Acknowledgement

We thank I. Nevoigt for carrying out the XRD measurements.

References

1. Han, H., et al., *The XBI BioLab for life science experiments at the European XFEL.* J Appl Crystallogr, 2021. **54**(Pt 1): p. 7-21.
2. Yan, Y., et al., *Fundamental Flaw in the Current Construction of the TiO2 Electron Transport Layer of Perovskite Solar Cells and Its Elimination.* ACS Appl Mater Interfaces, 2021. **13**(33): p. 39371-39378.
3. M. J. Frisch, G.W.T., H. B. Schlegel, G. E. Scuseria, , et al., *Gaussian 09, Revision D.01*. 2013, Gaussian, Inc.: Wallingford CT.
4. Marasinghe, P.A.B. and G.D. Gillispie, *Structure of 1,5-dihydroxyanthraquinone: a redetermination.* Acta Crystallographica Section C Crystal Structure Communications, 1993. **49**(1): p. 113-114.